COMMUNICATION

What's Inside the Box? – Length-Scales that Govern Fracture Processes of Polymer Fibers

*Tristan Giesa, Nicola M. Pugno, Joyce Y. Wong, David L. Kaplan, and Markus J. Buehler**

The fracture strength of natural fibers remains a topic of intense debate, as it has not yet been possible to predict their fracture strength directly from an atomistic point of view.[1] Here we show that the considerations of interatomic interactions alone cannot explain the fracture strength observed in biological fibers. Instead, the fracture strength of a fiber depends strongly on the length-scale of observation, and structures at multiple length-scales must be considered to explain their remarkable mechanical performance and resilience, including a fiber's sensitivity with respect to cracks (and other flaws). The impact of such stress concentrators on a material's performance was first quantified by Griffith and Weibull.[2] They developed strong theoretical arguments to explain the experimentally observed scaling of strength with specimen size, where smaller tends to be stronger, suggesting that the probability of having a critical flaw decreases with specimen size.

The fracture analysis of polymers is commonly addressed from two points of view: a statistical, micromechanical (e.g., using Bell theory or atomic potentials)[3] or a continuum mechanical (e.g., using phase field theory or linear/nonlinear fracture mechanics based on Griffith's work).[4] Both approaches are well explored, but are yet to be unified in a comprehensive framework. Our work provides a step towards this framework by connecting the characteristic length scales in hierarchical biological fibrous materials to their fracture strength from the level of the interatomic potential upwards, to characterize the fracture properties at the macroscopic scale.

Consider a polymer fiber of diameter D with no intrinsic flaws (**Figure 1**a). Under applied tension σ_0, such a fiber's failure strength σ_f would reach the theoretical limit of the interatomic bonds it consists of, denoted by σ_{th}. Similarly, one could consider a fiber with a distribution of intrinsic flaws. Such a fiber would fail at a finite 'macroscopic' strength. In contrast, a fiber made of the same bonds but containing a large flaw will significantly decrease its strength according to Griffith's size scaling,[2a,5] where the crack size scales with the diameter, such that $\sigma_f \sim 1/\sqrt{D}$.

The process zone, also depicted schematically in Figure 1b, characterizes the amount of material that contributes to resisting fracture, and is also referred to as the "cavitation box".[1a] It can be understood as the region surrounding a crack that is damaged during crack propagation. In the limit of a very small process zone (Figure 1b), on the order of atomic bonds, the material is very brittle like glass and bonds simply snap to create new surfaces. In the limit of a very large process zone (Figure 1c), driving a crack through the material leads to widespread damage that is not limited to the crack surface. An important aspect of a large process zone is that stress concentrations at the crack tip are diminished, further reducing the threat imposed by cracks of causing catastrophic damage to a material.

T. Giesa, Prof. M. J. Buehler
Laboratory for Atomistic and Molecular Mechanics
Department of Civil and Environmental Engineering
Massachusetts Institute of Technology
77 Mass. Ave. Room 1-235A&B, Cambridge,
MA, 02139, USA
E-mail: mbuehler@mit.edu
Prof. N. M. Pugno
Laboratory of Bio-Inspired & Graphene Nanomechanics
Department of Civil, Environmental and Mechanical Engineering
Università di Trento
Via Mesiano, 77, I-38123, Trento, Italy
Prof. N. M. Pugno
Center for Materials and Microsystems
Fondazione Bruno Kessler
Via Sommarive, 18, I-38123, Trento, Italy
Prof. J. Y. Wong
Department of Biomedical Engineering
Boston University
44 Cummington Mall, Boston, MA, 02215, USA
Prof. D. L. Kaplan
Department of Biomedical Engineering
Tufts University
Medford, MA, 02155, USA

DOI: 10.1002/adma.201303323

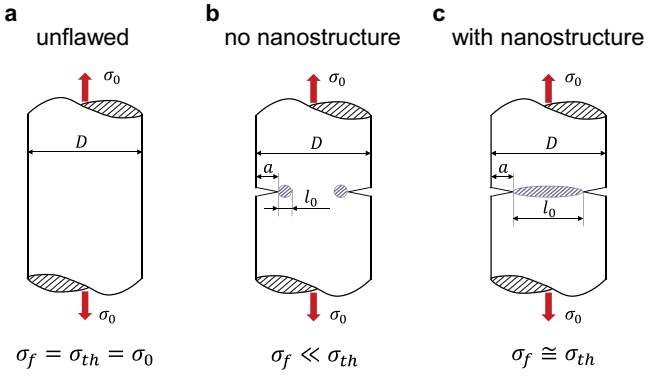

Figure 1. (a) A fiber of diameter D that has no intrinsic flaws. Under tension σ_0, such a fiber's failure strength σ_f would reach the theoretical strength of the interatomic bonds it consists of, σ_{th}. (b) A fiber made of the same bonds without internal structure but containing a flaw of length a would decrease its strength according to Griffith's size scaling as the ratio l_0/D and the strength of the fiber become smaller. (c) A possible strategy to maintain the strength of the fiber at the macroscale is to increase the size of the process zone (the "cavitation box"), such that $l_0 \approx D$. Then, the strength of the fiber will approach the theoretical strength of the internal structure, $\sigma_f \cong \sigma_{th}$.

The process zone size, characterized by the length-scale l_0, is indicative of the fracture toughness K of the fiber,[6] since $K \sim \sqrt{l_0}$.[7] This makes intuitive sense because dissipative processes that increase the size of the process zone will thereby lead to a larger fracture resistance of polymeric fibers. For example, self-healing processes (via H-bond stick-slip or hidden length in molecular domains) can increase the toughness during fracture. In addition to molecular processes, distributed failure processes can encompass microcracking, crack bridging, crack-deflection, as well as interfacial sliding (e.g., shearing of interfaces and unfolding of organic matrices).[1b,8]

How can we identify the process zone size l_0? In most cases, it can be measured by experimental analysis only. Some progress has been made from a continuum mechanical point of view.[9] One can estimate the process zone size l_0 from the ratio between a materials fracture strength σ_f and its yield strength σ_Y (defined as the stress where the material undergoes irreversible, plastic deformation),[10]

$$l_0 = \beta \left(\frac{\sigma_f}{\sigma_Y} \right)^2, \tag{1}$$

where β is proportional to the crack size, depends (for example) on the specimen geometry, and can include nonlinear geometric effects. This scaling law reflects the importance of the nonlinear nature of the stress-strain relationship as a means to decouple the failure stress from the yield stress. However, this does not provide an immediate route to predict l_0, because the ratio of failure to yield stress is not generally known. Starting from experimental observations, we will systematically address this question from the level of the interatomic potential upwards.

Experimental Observations: For many biomaterials, the process zone size l_0 has been experimentally determined to be on the order of several micrometers, *e.g.* for bone,[8d,11] polymers,[12] and quasibrittle materials.[13] The process zone has also been directly measured in concrete, graphite, and wood via acoustic emission, digital imaging, and SEM.[14] In these studies, the damage zone surrounding the crack tip was visually identified as process zone. In a recent paper, empirical relations were used to estimate the process zone size l_0 in spider silk and other polymeric fibers, and found to be on the order of one micrometer.[1a,15] To obtain this result, the authors invoked an empirical scaling relation that relates the yield stress to the elastic properties via $\sigma_Y = 0.028E$. As other analyses, this study did not describe the fracture properties of fibers from a fundamental, interatomic potential point of view, but rather lumped a variety of mechanisms into an empirical equation that ultimately relates the yield strength to the fracture strength.

Atomistic Perspective: We estimate the process zone size directly from an interatomic potential. This fundamental approach accounts for the fact that fracture involves the rupture of atomic bonds. The generalized Lennard-Jones (n, m) potential (LJ) is often used as an approximation for the behavior of interatomic interactions in polymers and crystalline materials (e.g., Ref. [16], and it therefore provides a good basis for the study of the fracture mechanisms in natural fibers.[17] An appropriate model to estimate the size of the process zone size l_0 from the interatomic potential is the Dugdale-Barenblatt yield-strip model, given by

$$l_0 = \frac{\pi}{8} E \frac{G_c}{\sigma_{th}^2}, \tag{2}$$

with G_c as the critical energy release rate, E the elastic modulus of the bonds, and σ_{th} the theoretical strength of a chemical bond.[18] For a nonlinear material, G_c can be generalized to [10]

$$G_c = \int_{r_0}^{\infty} \sigma(r)\, dr \tag{3}$$

where r_0 is the equilibrium lattice spacing of a cubic lattice on which the molecules are arranged (detailed derivation see Experimental Section and Methods). Solving Equation (2) yields the ratio of process zone size to the characteristic length scale r_0, with $l_0/r_0 = f(n, m)$. Here, $f(n, m)$ is a function of the parameters of a generalized Lennard-Jones-potential. It is found that l_0/r_0 is relatively insensitive to the parameters (n, m), see **Table 1**. Estimating an upper and lower bound for this ratio yields an interval of $l_0/r_0 \approx [0.5, 16]$, or [0.25 nm, 8 nm] for most real materials. An important observation from this derivation is the existence of a relation between characteristic length scale r_0 and process zone size l_0, which is in turn directly connected to the fracture toughness of the material. On the level of chemical bonds, one can think of r_0 as the "lattice" spacing in the strong and often ordered polymer domains. In strong and tough protein or polymer fibers this refers to the inter-chain distance in highly aligned β-sheets (e.g., nylon, amyloids, spider dragline MaSp1 and silkworm silks, strained collagen, titin-rich myofibrils, and some synthetic polymers),[19] α-helices (e.g., intermediate filaments, actin fibers), or β-turns (e.g., silk MaSp2, elastin and some synthesized polymer fibers).[20] Note the ratio l_0/r_0 depends on the actual lattice structure present in the material (details, see Experimental Section and Methods) and on the specific make-up of its substructure, as well as other effects such as orientation and temperature. In view of the generality of our analysis and the purpose of obtaining an order of magnitude estimate, this is considered negligible.

Our predictions are in good agreement with several earlier reports. For soft elastic materials, Hui et al. estimated the size of the process zone to be approximately 1 nm.[21] Similarly, Porter et al. derived the process zone size l_0 for silk materials to be around 4 nm.[22] Keten et al. investigated the fracture behavior of hydrogen bond clusters, found in many secondary structural elements of (semi-)crystalline polymer fibers,[23] leading to a process zone size of approximately 1 nm.[24] Generally, this analysis holds not only for polymeric fibers but also for metals or ceramics. In sum, the calculation based on the LJ potential results in exceedingly small sizes on the order of a few

Table 1. Process zone (cohesive zone) for the generalized LJ potential.

n	m	l_0/r_0
12	6	0.5–10
12	8	0.4–9.2
10	2	1.0–16

nanometers. Consequently, this suggests a low fracture toughness (as $K \sim \sqrt{l_0}$), in contrast to the experimental results, which we will address in the next section.

Connecting the Length Scales: How is it possible that polymer materials show dramatically higher fracture toughnesses than predicted by the preceding atomistic analysis, with a remarkable mismatch by a factor of 1000? This contradiction can be explained by Equation (1). Considering the purely elastic nature of the potential up to failure, the ratio between yield strength σ_Y and fracture strength $\sigma_f = \sigma_{th}$ of a LJ material is approximately one, i.e., $\sigma_f \approx \sigma_Y$ (or close to it).[25]

In order to achieve a very large process zone size the yield stress and fracture strength must be decoupled. As we have shown this cannot be achieved in a homogeneous material and therefore the existence of a heterogeneous material microstructure is critical. Spider silk's heterogeneity, for example, is caused by a composite arrangement of alanine rich nanocrystals within a glycine rich semi-amorphous phase (for a detailed description, see Ref. [26]). Other well-known examples that incorporate such complex microstructural architectures are wood, bone, glassy sponges, nacre, and tendons, to name a few.[8b]

In such structures, the characteristic length scale r_0 is not a material constant, but depends on the length scale of observation.[27] **Figure 2** depicts this concept in the context of spider dragline silk. On the lowest hierarchical level, the scale of the atomic bonds, the maximum stress is the theoretical bond stress σ_{th} r_0 and l_0 are small. Therefore, a strong and tough fiber requires a nanoscale substructure that has dimensions of the process zone size in order to be robust at larger scales. In spider silk, nanocrystals constitute this substructure with dimensions of 2–4 nanometers.[26,28] On the next hierarchical level, the beta-sheet crystals form a structure that can be understood as a lattice with spacing of $r_0 \approx 10\text{nm}$, the distance between the crystals (note how r_0 changes with the length scale of observation).

The intrinsic strength of the lower scale feature – here the crystal and amorphous phase – is scaled up to the next larger scale. Paired with the unfolding of the semi-amorphous protein domains, the process zone size is then of the order of 20–150 nm, the size of the fibrils.[29] This is in agreement with the estimate of the process zone size $l_0/r_0 \approx [0.5, 16]$. The importance of spider silks heterogeneity in connection with these length scales has been intensively studied using SEM, X-Ray and neutron scattering techniques.[30] Through hierarchical assembly, i.e., the weak binding of many layers of flaw-tolerant fibrils to fibers, the material induces further toughening mechanisms (fibril sliding and delocalization) and maintains its toughness at micrometer dimensions.[31] This shows that the resilience of materials is greatly enhanced through hierarchical structure originating at the nanoscale, as deformation and damage processes become translated to larger scales.[32] A similar setup can be found in the cellulose fibers in wood, where an arrangement of nanocrystals forms nanometer-sized microfibrils that are densely packed into a lattice like structure.[33] Also collagen (e.g., in bone and mussel threads), keratin-based materials, chitin-protein fibers and their derivatives contain highly repetitive patterns on several length scales that can be interpreted as a lattice with spacing r_0.[34] The concept is schematically shown in **Figure 3** for a general case. The

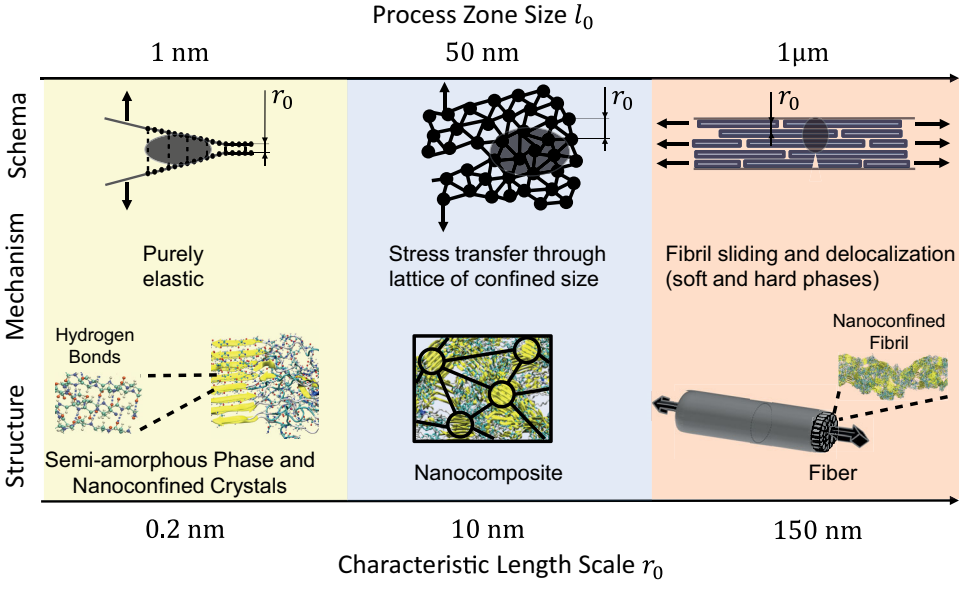

Figure 2. Length scales and toughening mechanisms in spider dragline silk. At the lowest hierarchical level, the scale of the atomic bonds, the maximum stress is the theoretical bond stress σ_{th} and r_0 as well as l_0 are small (in the order of nanometers). The nanocrystal is extremely robust because it is geometrically confined to the size of the plastic zone. At the next hierarchical level, the beta-sheet crystals form a structure that can be understood as a lattice with spacing of $r_0 \approx 10$ nm, the distance between the crystals. The intrinsic strength of the lower scale feature – here the crystal and amorphous phase – is scaled up to the next scale. Paired with the unfolding of the semi-amorphous protein domains, the process zone size is then on the order of 20–150 nm, the size of the fibrils. Through hierarchical assembly, i.e., the weak binding of many layers of flaw-tolerant fibrils to fibers, the material induces further toughening mechanisms (fibril sliding and delocalization, inducing a process zone of 1 μm) and maintains its toughness at micrometer dimensions.

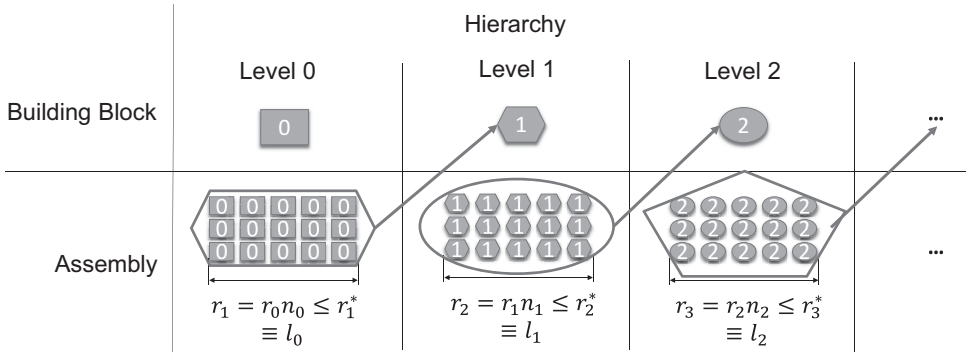

Figure 3. Schematic picture of the hierarchical build-up of materials, where at each level the building blocks are repeated n times such that the total length is confined to r^*. At each hierarchical scale, the stress concentrations become delocalized. This is achieved through the confinement of each microstructure to the length scale of the process zone size $l_0/r_0 =$ [0.5, 16], where r_0 is the characteristic size of the building block. The fiber becomes robust to flaws at all these length scales and does not fail in a brittle manner, when part of a larger-scale hierarchical structure. The resilience of materials is greatly enhanced through hierarchical structuring from the nanoscale upwards, as deformation and damage processes are translated to larger scales.

fiber becomes robust to flaws at all these length scales and does not fail in a brittle manner, when part of a larger-scale hierarchical structure. This is achieved through the confinement of each microstructure to the length scale of the process zone size (called r^* in Figure 3), governed by $l_0/r_0 \approx [0.5, 16]$, where r_0 is the characteristic size of the length scale under observation.

In spider silk, the onset of failure in the early deformation stages of the weakly bonded semi-amorphous phase controls the nonlinear softening after the elastic regime.[26b,35] This constitutes a yield mechanism where $\sigma_Y \approx (1/4)\,\sigma_f$.[35,36] A general observation of great importance is that spider silk features a very small yield stress and at the same time, a very large fracture stress. This leads to a very large process zone size on the order of 300 nm to 1000 nm (see Supporting Information). The key to these considerations is that the particular nonlinear stress-strain relationship in silk fibers originates from a hierarchical arrangement of distinct components, starting at the nanoscale.[39] Beyond the specific case of silk, the strategy to achieve large process zones is ubiquitous in many natural materials,[37,40] where strong nanoconfined constituents (in fibers: crystallized fibrils, in composites: platelets) are bound by a weak matrix (in fibers: weak chain interactions, in composites: a weak polymer phase).

In summary, we showed the existence of an intrinsic mismatch between the length-scales involved in the fracture mechanics of biological materials, and applied a simple model to connect the interatomic potential to the fracture toughness of hierarchical materials. To achieve this we used fracture mechanics and derived the process zone size. We found that without considering hierarchical structures, the size of the process zone derived from the atomistic scale is only a few nanometers, constituting a mismatch by up to factor 1000. By incorporating a hierarchy of structures, each confined to a certain critical length-scale, we were able to explain the process zone size observed in experimental observations and link it directly to an interatomic potential.

We found that the scaling law for the strength of a material and also the related experimental and theoretical analysis are universal throughout all length scales. What matters is the interpretation of the parameters, which differs between the nano- and the macroscale. We also found that the nanostructure is fundamental to the mechanisms that transfer the strength from atomic bonds to the macroscopic fiber. This paradigm could provide an answer to the longstanding question how natural fibers scale up the nanoscale strength to the experimentally observed high strength, extensibility and robustness. This insight provides a path towards new material designs by embracing hierarchical structures.

Experimental Section and Methods

Derivation of the process zone size for a generalized Lennard-Jones potential: The generalized LJ-(n, m)-potential formulation is given by

$$\Phi(r, n, m) = \omega\left[\frac{m}{n-m}\left(\frac{r_0}{r}\right)^n - \frac{n}{n-m}\left(\frac{r_0}{r}\right)^m\right]. \tag{A1}$$

Here, r_0 is the equilibrium bond distance, r the current bond distance, and ω, n, m potential parameters. Similar to the derivation in Ref. [17a], one finds for this potential the strain energy density

$$\Psi = \frac{\Phi}{\Omega}, \tag{A2}$$

the stress-displacement function with $\sigma = \partial\Psi/\partial\varepsilon$, where $\varepsilon = (r - r_0)/r_0$ is the bond strain,

$$\sigma(r, n, m) = \frac{nm\omega}{(n-m)\Omega}\left[-\left(\frac{r_0}{r}\right)^{n+1} + \left(\frac{r_0}{r}\right)^{m+1}\right], \tag{A3}$$

and the elastic modulus $E = \partial^2\Psi/\partial\varepsilon^2$,

$$E(r, n, m) = \frac{nm\omega}{(n-m)\Omega}\left[(n+1)\left(\frac{r_0}{r}\right)^{n+2} - (m+1)\left(\frac{r_0}{r}\right)^{m+2}\right], \tag{A4}$$

with Ω as the bond volume.

The theoretical attainable bond stress is given by setting $E = 0$,

$$\sigma_{th}(n, m) = \frac{nm\omega}{\Omega(n+1)}\left(\frac{m+1}{n+1}\right)^{\frac{m+1}{n-m}}. \tag{A5}$$

Furthermore, the cohesive energy, which equals the fracture surface energy of the bond, is given by

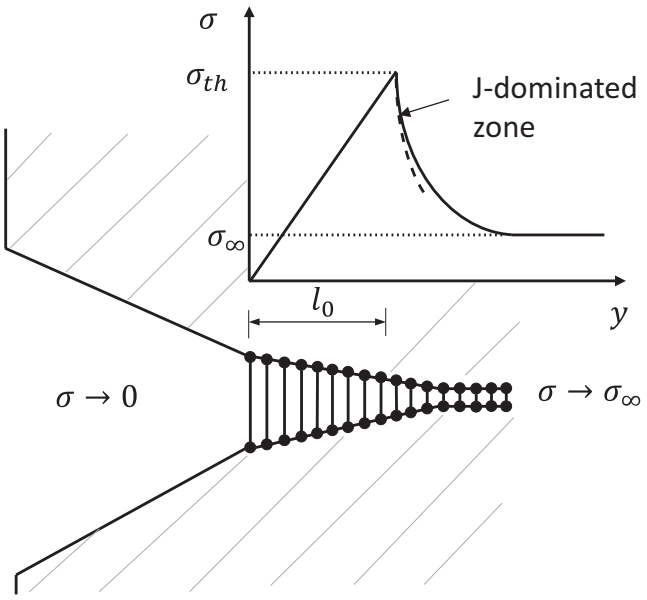

Figure 4. Stress variation in the cohesive zone according to the Dugdale-Barenblatt model.

$$\gamma_s = \int_{r_0}^{\infty} \sigma(r)\, dr = \frac{\omega r_0}{\Omega}. \tag{A6}$$

These definitions have been reported in Ref. [17a]. To the best of the authors' knowledge, the following derivation has not been reported in literature.

An appropriate model to estimate the size of the decohesion or process zone l_0 is given by the Dugdale-Barenblatt yield-strip model, see **Figure 4**,

$$l_0 = \frac{\pi}{8} E \frac{G_c}{\sigma_{th}^2}, \tag{A7}$$

where G_c is the critical energy release rate, a material parameter that quantifies the amount of energy needed to drive a crack through a surface.[38]

Usually, derivations for nonlinear constitutive behavior entail a linearization of the elastic modulus around $\varepsilon = 0$ (i.e., $r = r_0$),[17a]

$$E_0(n, m) = \frac{nm\omega}{\Omega}. \tag{A8}$$

The modulus as it appears in Equation (A7) is the modulus of the stress far field, to account for the change in strain energy in the specimen upon crack propagation. In a very large specimen, it is reasonable to set $E = E_0$. However, if the specimen size is small, in the order of the plastic zone, then $E \neq E_0$. This is the case for nanoconfined constituents in many biological materials, *e.g.* the fibrils in spider dragline silk or cellulose fibrils in wood.[37] In many nonlinear elastic material models, the stress behind the crack tip degrades with close to $1/\sqrt{r}$, similar to the linear elastic case. This implies that the material within a zone of 3-5 times the crack size (can be estimated from fracture mechanics, here without proof) has a much lower modulus than the far field. In a nano-sized material, this zone can contain the entire specimen. To account for the highly nonlinear behavior in the cohesive zone, it seems more appropriate to calculate an average elastic modulus that averages from the crack tip, $E = 0$, to the linearized modulus $E = E_0$.

$$\bar{E}(n, m) = \frac{nm\omega}{\Omega (n+1) \left(\frac{n+1}{m+1}\right)^{\frac{m+1}{n-m}}} = \sigma_{th}(n, m) \tag{A9}$$

Most materials have a modulus that is higher than the theoretical strength, so the estimate $E = \bar{E}$ will serve as a lower bound for the process zone size l_0 in Equation (A7).

Due to the elastic nature of the potential, G_c can be simplified to

$$G_c = \gamma_s + \int_0^{l_0} \left(\int_0^{\varepsilon_{ij}} \sigma_{ij}\, d\varepsilon_{ij} \right) dy = \gamma_s. \tag{A10}$$

Now, we can write an expression for the plastic zone size only in terms of the bond potential parameters using Equation (A7). The lower bound for l_0 is given by the averaged modulus in Equation (A10),

$$l_{0,\bar{E}} = \frac{\pi (n+1) \left(\frac{m+1}{n+1}\right)^{-\frac{m+1}{n-m}}}{8\, nm} r_0. \tag{A11}$$

Alternatively, using the linearized expression of the elastic modulus, Equation (A9), we obtain an upper bound for l_0,

$$l_{0,E_0} = \frac{\pi (n+1)^2 \left(\frac{m+1}{n+1}\right)^{-2\frac{m+1}{n-m}}}{8\, nm} r_0. \tag{A12}$$

The results are summarized in Table 1 for typical combinations of parameters (n, m). The values for l_0 aremonly a function of (n, m) and the bond distance r_0. Note that this assumes a 1-D arrangement of bonds, for example found on the nanoscale in β-sheets. For a lattice-like arrangement one would need to sum over the contributions from several bonds, which would lead to an increase in l_0. For the purpose of this paper, an order of magnitude estimation, the simple 1-D analysis is sufficient.

Supporting Information

Supporting Information is available from the Wiley Online Library or from the author.

Acknowledgements

TG, JW, DK and MJB are supported by NIH U01/EB014976. NMP is supported by the European Research Council (ERC StG 2011 BIHSNAM on "Bio-inspired hierarchical super-nanomaterials") and ERC Proof of Concept REPLICA. MJB and TG acknowledge additional support from ARO (W991NF-09-1-0541).

Received: July 18, 2013
Published online: November 11, 2013

[1] a) D. Porter, J. Guan, F. Vollrath, *Adv. Mater.* **2012**, *25*, 1275; b) H. J. Gao, *Int. J. Fracture* **2006**, *138*, 101.

[2] a) A. A. Griffith, *Philos. Trans R. Soc. A* **1921**, *221*, 163; b) W. Weibull, *J. Appl. Mech.-T ASME* **1951**, *18*, 293.

[3] a) I. G. Salib, G. V. Kolmakov, B. J. Bucior, O. Peleg, M. Kroger, T. Savin, V. Vogel, K. Matyjaszewski, A. C. Balazs, *Langmuir* **2011**, *27*, 13796; b) A. G. Mikos, N. A. Peppas, *J. Chem. Phys.* **1988**, *88*, 1337.

[4] a) C. Miehe, L.-M. Schaenzel, *J. Mech. Phys. Solids* **2013**, http://dx.doi.org/10.1016/j.jmps.2013.06.007; b) M. A. Meyers, K. K. Chawla, *Mechanical behavior of materials*, Cambridge University Press, Cambridge, New York **2009**; c) J. G. Williams, *Fracture mechanics of polymers*, E. Horwood; Halsted Press, Chichester, New York **1984**; d) P. P. Camanho, M. A. Bessa, G. Catalanotti, M. Vogler, R. Rolfes, *Mech. Mater.* **2013**, *59*.

[5] a) H. J. Gao, B. H. Ji, I. L. Jager, E. Arzt, P. Fratzl, *Proc. Natl. Acad. Sci. USA* **2003**, *100*, 5597; b) M. J. Buehler, H. M. Yao, H. J. Gao, B. H. Ji, *Model. Simul. Mater. Sci. Eng.* **2006**, *14*, 799.
[6] a) Z. P. Bazant, *Proc. Natl. Acad. Sci. USA* **2004**, *101*, 13400; b) H. B. Chen, J. S. Wu, *Macromolecules* **2007**, *40*, 4322.
[7] M. F. Ashby, A. L. Greer, *Scri. Mater.* **2006**, *54*, 321.
[8] a) H. Peterlik, P. Roschger, K. Klaushofer, P. Fratzl, *Nat. Mater.* **2006**, *5*, 52; b) P. Fratzl, R. Weinkamer, *Prog. Mater. Sci.* **2007**, *52*, 1263; c) R. O. Ritchie, *Nat. Mater.* **2011**, *10*, 817; d) M. E. Launey, M. J. Buehler, R. O. Ritchie, *Annu. Rev. Mater. Res.* **2010**, *40*, 25.
[9] a) J. R. Rice, *J. Appl. Mech.* **1968**, *35*, 379; b) M. Brunig, *Int. J. Mech. Sci.* **2004**, *46*, 1763; c) N. M. Pugno, R. S. Ruoff, *Philos. Mag.* **2004**, *84*, 2829; d) T. Giesa, M. Arslan, N. M. Pugno, M. J. Buehler, *Nano Lett.* **2011**, *11*, 5038.
[10] T. L. Anderson, *Fracture mechanics: fundamentals and applications*, Taylor & Francis, Boca Raton, FL **2005**.
[11] a) D. M. Robertson, D. Robertson, C. R. Barrett, *J. Biomech.* **1978**, *11*, 359; b) J. J. Kruzic, D. K. Kim, K. J. Koester, R. O. Ritchie, *J. Mech. Behav. Biomed. Mater.* **2009**, *2*, 384.
[12] a) C. S. Litteken, R. H. Dauskardt, *Int. J. Fracture* **2003**, *119*, 475; b) O. Bougaut, D. Rittel, *Int. J. Solids Struct.* **2001**, *38*, 2517; c) D. Rittel, *Int. J. Fracture* **1999**, *99*, 199; d) J. S. Wu, Y. W. Mai, *Polym. Eng. Sci.* **1996**, *36*, 2275.
[13] a) A. G. Evans, K. T. Faber, *J. Am. Ceram. Soc.* **1984**, *67*, 255; b) Z. P. Bazant, G. Pijaudiercabot, *J. Eng. Mech.-ASCE* **1989**, *115*, 755.
[14] a) L. Cedolin, S. D. Poli, I. Iori, *Cement Concrete Res.* **1983**, *13*, 557; b) S. P. Shah, S. Choi, *Int. J. Fracture* **1999**, *98*, 351; c) S. Nakhodchi, A. Hodgkins, R. Moskovic, D. J. Smith, P. E. J. Flewitt, *Key Eng. Mater.* **2011**, *452-453*, 93; d) I. Smith, S. Vasic, *Mech. Mater.* **2003**, *35*, 803.
[15] J. T. Seitz, *J. Appl. Polym. Sci.* **1993**, *49*, 1331.
[16] A. Grzybowski, K. Koperwas, M. Paluch, *Phys. Rev. E* **2012**, *86*.
[17] a) R. Ballarini, R. Kayacan, F. J. Ulm, T. Belytschko, A. H. Heuer, *Int. J. Fracture* **2005**, *135*, 187; b) Y. K. Kang, *J. Phys. Chem. B* **2000**, *104*, 8321.
[18] a) D. S. Dugdale, *J. Mech. Phys. Solids* **1960**, *8*, 100; b) J. G. Williams, H. Hadavinia, *J. Mech. Phys. Solids* **2002**, *50*, 809.
[19] a) C. Meier, M. E. Welland, *Biomacromolecules* **2011**, *12*, 3453; b) A. M. Kushner, J. D. Vossler, G. A. Williams, Z. B. Guan, *J. Am. Chem. Soc.* **2009**, *131*, 8766.
[20] J. E. Jenkins, M. S. Creager, E. B. Butler, R. V. Lewis, G. P. Holland, J. L. Yarger, *Chem. Commun.* **2010**, *46*, 6714.
[21] C. Y. Hui, A. Jagota, S. J. Bennison, J. D. Londono, *Proc. R. Soc. London, Ser. A* **2003**, *459*, 1489.
[22] D. Porter, F. Vollrath, *Adv. Mater.* **2009**, *21*, 487.
[23] S. Keten, M. J. Buehler, *Phys. Rev. Lett.* **2008**, *100*, 198301.
[24] S. Keten, M. J. Buehler, *Nano Lett.* **2008**, *8*, 743.
[25] F. Varnik, L. Bocquet, J. L. Barrat, *J. Chem. Phys.* **2004**, *120*, 2788.
[26] a) S. Keten, Z. P. Xu, B. Ihle, M. J. Buehler, *Nat. Mater.* **2010**, *9*, 359; b) A. Nova, S. Keten, N. M. Pugno, A. Redaelli, M. J. Buehler, *Nano Lett.* **2010**, *10*, 2626.
[27] P. Cornetti, N. Pugno, A. Carpinteri, D. Taylor, *Eng. Fract. Mech.* **2006**, *73*, 2021.
[28] D. T. Grubb, L. W. Jelinski, *Macromolecules* **1997**, *30*, 2860.
[29] N. Du, X. Y. Liu, J. Narayanan, L. A. Li, M. L. M. Lim, D. Q. Li, *Biophys. J.* **2006**, *91*, 4528.
[30] a) F. Vollrath, T. Holtet, H. C. Thogersen, S. Frische, *Proc. R. Soc. London. Ser. B* **1996**, *263*; b) C. Riekel, F. Vollrath, *Int. J. Biol. Macromol.* **2001**, *29*, 203; c) F. Vollrath, D. P. Knight, *Nature* **2001**, *410*, 541; d) F. Vollrath, D. Porter, *Soft Matter* **2006**, *2*, 377; e) D. Sapede, T. Seydel, V. T. Forsyth, M. A. Koza, R. Schweins, F. Vollrath, C. Riekel, *Macromolecules* **2005**, *38*, 8447.
[31] L. S. Dimas, T. Giesa, M. J. Buehler, *J. Mech. Phys. Solids* **2013**, http://dx.doi.org/10.1016/j.jmps.2013.07.006.
[32] T. Giesa, N. M. Pugno, M. J. Buehler, *Phys. Rev. E* **2012**, *86*, 041902.
[33] A. N. Fernandes, L. H. Thomas, C. M. Altaner, P. Callow, V. T. Forsyth, D. C. Apperley, C. J. Kennedy, M. C. Jarvis, *Proc. Natl. Acad. Sci. USA* **2011**, *108*, E1195.
[34] a) M. A. Meyers, P. Y. Chen, A. Y. M. Lin, Y. Seki, *Prog. Mater. Sci.* **2008**, *53*, 1; b) J. Jin, P. Hassanzadeh, G. Perotto, W. Sun, M. A. Brenckle, D. Kaplan, F. G. Omenetto, M. Rolandi, *Adv. Mater.* **2013**, *25*, 4482; c) A. Hagenau, H. A. Scheidt, L. Serpell, D. Huster, T. Scheibel, *Macromol. Biosci.* **2009**, *9*, 162.
[35] S. Keten, M. J. Buehler, *J. R. Soc. Interface* **2010**, *7*, 1709.
[36] a) I. Agnarsson, M. Kuntner, T. A. Blackledge, *PloS One* **2010**, *5*; b) F. Vollrath, D. Porter, *Appl. Phys. A: – Mater. Sci. Process.* **2006**, *82*, 205.
[37] T. Giesa, M. J. Buehler, *Annu. Rev. Biophys.* **2013**, *42*, 651.
[38] H. Tada, P. C. Paris, G. R. Irwin, *The stress analysis of cracks handbook*, ASME Press, New York **2000**.
[39] F. G. Omenetto, D. L. Kaplan, *Science* **2010**, *329*, 528.
[40] M. A. Lillie, J. M. Gosline, *Int. J. Biol. Macromol.* **2002**, *30*, 119.